Indonesian Physical Review
Volume 08 Issue 03, September 2025
P-ISSN: 2615-1278, E-ISSN: 2614-7904

Design and Characterization of a Simple Temperature Sensor Based on a Polymer Sine S-Bend Optical Waveguide Structure

Ian Yulianti*, Rizki Roqissatul Hidayah, Joshu Leonardy, Fianti, Sunarno, Wasi Sakti W. P, Galih R. Utomo, Defrian Prayogo, Nishfa Mufatihah
Physics Study Program, Faculty of Mathematics and Natural Sciences, Universitas Negeri Semarang, Indonesia

Corresponding Author's E-mail: ianyulianti@mail.unnes.ac.id

Article Info

Article info:
Received: 28-05-2025
Revised: 18-09-2025
Accepted: 22-09-2025

Keywords:
Temperature sensor; S-bend; Optical waveguide; PMMA; UPR.

How To Cite:
I. Yulianti. R. R. Hidayah, J. Leonardy, Fianti, Sunarno, W. Sakti, G. R. Utomo, D. Prayoga, and N. Mufatihah, "Design and Characterization of a Simple Temperature Sensor Based on a Polymer Sine S-Bend Optical Waveguide Structure", Indonesian Physical Review, vol. 8, no. 3, p 771-789, 2025

DOI:
https://doi.org/10.29303/ipr.v83.511.

Abstract

This study presents the design, fabrication, and performance evaluation of a sine S-bend embedded square-core optical waveguide for temperature sensing applications. The waveguide was fabricated using a straightforward and cost-effective CNC milling technique, with PMMA as the cladding and unsaturated polyester resin (UPR) as the core material. Three different bend heights (0.5 cm, 0.6 cm, and 0.7 cm) were investigated to assess their effects on sensor sensitivity, response time, accuracy, and hysteresis. Results showed that increasing the bend height enhanced the sensor sensitivity, with the highest sensitivity of 0.0283 dB/°C achieved at a bend height of 0.7 cm. The response time was consistently maintained at approximately 40 seconds across all samples. The sensor exhibited excellent accuracy, reaching up to 99.31% at a bend height of 0.5 cm. The maximum hysteresis observed was 0.202 % at a bend height of 0.7 cm, indicating stable performance during thermal cycling. These results confirm that the integration of a sine S-bend structure, smooth core surface, and precise waveguide dimensions can significantly improve sensor performance while maintaining a simple and scalable fabrication process.

Introduction

Optical waveguides are critical components in photonic systems to confine and guide light, which could be found in applications such as telecommunications [1, 2] and sensing technologies [3- 6]. Waveguides can be fabricated in various configurations, including planar, rib, and ridge, with a wide range of materials such as silica [7] and polymers [8]. Their compact size, scalability, and high precision have positioned optical waveguides as a cornerstone in the advancement of modern photonic devices.

In sensor applications, optical waveguides are valued for their ability to detect changes in environmental parameters through variations in light intensity, phase, or wavelength. For temperature sensing, waveguides leverage the thermo-optic effect or refractive index changes caused by temperature variations, enabling precise and rapid measurements. Polymer waveguides are known for their high thermo-optic coefficients, which enhance sensitivity, while silica waveguides offer excellent thermal stability and robustness. Several studies have demonstrated waveguide-based temperature sensors. Gao et al. [9] proposed a polymer-silica hybrid Mach-Zehnder interferometer (MZI) waveguide to enhance sensor sensitivity. Another MZI-based waveguide temperature sensor was demonstrated by Deng et al. [10], featuring a composite optical waveguide (COW) sandwiched between two single-mode fibers (SMFs). However, these designs face challenges related to fabrication complexity. A simpler fabrication approach was demonstrated by Davila et al. [11], utilizing the temperature-dependent fluorescence of rhodamine B doped into the waveguide core. Despite its straightforward fabrication technique, this sensor requires a complex detection mechanism to accurately measure the wavelength shift.

A simple detection mechanism optical sensor can be realized using the intensity modulation technique. The fundamental principle of the intensity modulation sensors relies on temperature-induced variations that modulate the intensity of light propagating. Various intensity modulated temperature sensors have been developed using Fiber Bragg Grating (FBG) [12], fluorescence method [13-15], and light field modulation [16]. Another notable method in intensity modulation optical sensors is the bending loss-based optical sensor, known for its high sensitivity. Remouche et al. [17] developed intensity modulation optical waveguide sensors by exploiting temperature-dependent loss in the bending region. As the bend becomes sharper or the curvature radius decreases, the sensor's sensitivity to temperature increases [18]. Gu et al. [19] used bended-dual core optical fiber and spot pattern for temperature detection. The results indicated that the sensor could detect varying temperatures within the range of 30–199 °C, with a resolution greater than 0.05 °C.

In addition to curvature waveguide, S-bend waveguide is a promising design for optical sensor since the structure has multiple bending regions, stronger evanescent wave leakage, and higher sensing sensitivity [20]. S-bend waveguide structures are widely used in optical devices to facilitate lateral displacements and smooth connections within integrated optical circuits. Various S-bend configurations have been explored in previous studies, such as the cosine S-bend [21], arc S-bend [22], and sine S-bend [23]. The curvature of a cosine S-bend follows a cosine function, which ensures a smooth transition of light through the bend, reducing propagation loss and insertion loss. However, the gradual curvature limits the enhancement of the evanescent field interaction, thereby reducing overall sensitivity. Arc S-bend design aims to balance the trade-off between minimizing bending loss and maintaining compact device dimensions. However, it introduces additional coupling loss due to the sharp transition between bends. The curvature of a sine S-bend follows a sine function, which provides a gradual transition of light through the bend. This minimizes abrupt transitions, reducing propagation loss while maintaining high sensitivity. The sine S-bend configuration allows for enhanced evanescent field interaction, improving sensitivity without sacrificing signal stability.

The implementation of S-bend optical waveguides for optical sensors has been reported in several studies. For instance, Zhao et al. [24] proposed S-bend waveguides for acetylene detection, while S-bend waveguides have also been developed for use as resonators in

refractive index sensors [25]. Despite these advantages, studies focusing specifically on the application of S-bend waveguides for temperature sensing remain limited, particularly in terms of optimizing their design for enhanced performance and investigating their behaviour under varying environmental conditions. Moreover, the implementation of S-bend waveguide-based optical sensors often faces significant fabrication challenges. Conventional fabrication approaches typically involve multiple complex steps, including deposition, photoresist spin coating, E-beam lithography, development, dry etching, and photoresist removal [26].

Building upon these observations, it is evident that although previous research has underscored the promising potential of S-bend waveguide structures—particularly sine S-bends—in enhancing evanescent field interaction and thereby improving sensor sensitivity, practical implementations in temperature sensing applications remain constrained. This is primarily due to the aforementioned fabrication complexities associated with realizing precise S-bend geometries, which often require costly, multi-step processes and specialized cleanroom facilities. Such limitations hinder rapid prototyping and large-scale production, restricting the widespread deployment of high-performance optical sensors in diverse environments. Therefore, there exists a clear need for the development of affordable, scalable, and easily manufacturable S-bend waveguide sensors that retain the performance advantages demonstrated in simulation studies. This work addresses that need by introducing a simple CNC-milled approach to fabricate sine S-bend waveguides using accessible polymer materials, thereby offering a low-cost yet effective alternative for temperature sensing applications.

In this study, we proposed an S-bend waveguide for a temperature sensor application, fabricated using a straightforward CNC milling technique. To provide higher sensitivity and more stable signal output compared to cosine or arc designs, the sine S-bend configuration was implemented [23]. An embedded square core waveguide was selected since the square geometry provides enhanced mode confinement compared to circular waveguides, improving light transmission efficiency and reducing propagation loss [27]. Moreover, square core waveguides can be fabricated using CNC milling, reducing complexity and production cost compared to photonic crystal or rib waveguides. Polymethyl Methacrylate (PMMA), a low-cost and readily available material, is used as the cladding, while unsaturated polyester resin (UPR) serves as the core material. PMMA/UPR optical waveguides have previously been studied for refractive index sensors [28], demonstrating their potential for precise environmental sensing. However, their use for temperature sensing remains largely unexplored. Leveraging the thermo-optic properties of PMMA and UPR in an S-bend structure offers a promising approach for developing a highly sensitive and stable temperature sensor. Furthermore, thermal studies of the PMMA/UPR waveguide have shown that it exhibits good thermal stability when exposed to temperatures up to 70 °C [29], reinforcing its potential for reliable temperature sensing applications.

Experimental Method

The first stage of this work was the fabrication of waveguides with various bend heights (h). The subsequent step involved characterizing the waveguide's surface quality and dimensions, as well as evaluating its sensitivity, response time, hysteresis, and accuracy. Finally, the results were analyzed, as summarized in the flow chart shown in Figure 1.

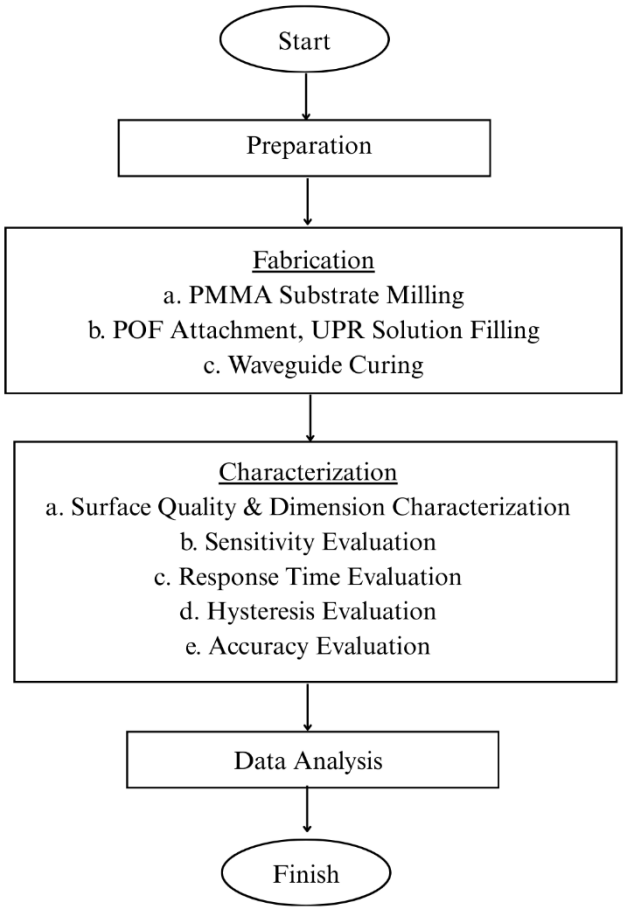

Figure 1. Flow chart of the waveguide sensor fabrication and characterization.

Fabrication of S-Bend Waveguide Sensor

The S-bend waveguide sensor was fabricated using a CNC milling technique to create the waveguide cladding from PMMA. The PMMA sheet was cut into dimensions of 4 × 2 cm with a thickness of 2 mm. The S-bend groove was milled with a depth of 1 mm based on the sinusoidal function, as defined in Equation (1) [30].

$$y(z) = \frac{h}{L}z - \frac{h}{2\pi}\sin\left(\frac{2\pi}{L}z\right) \quad (1)$$

where h is the bend height, L is the bend length, and z is the distance along the longitudinal direction. Three samples were prepared with varying bend heights of 0.5 cm, 0.6 cm, and 0.7 cm. Meanwhile, the bend length was maintained at 2 cm. The waveguide geometry is shown in Figure 2.

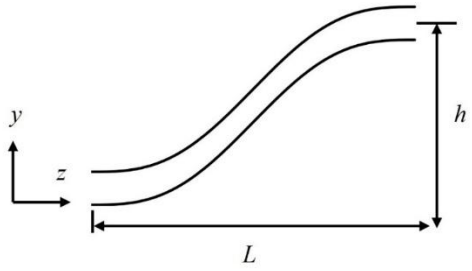

Figure 2. Sine S-bend waveguide geometry.

Figure 3 illustrates the fabrication process of the S-Bend waveguide. The core material was prepared by mixing UPR with Methyl Ethyl Ketone Peroxide (Mepoxe) as a crosslinking agent in a 400:1 ratio. The UPR solution was stirred with a magnetic stirrer at 60 rpm at room temperature until the UPR was completely dissolved [29]. Plastic optical fibers (POFs) were connected at both ends of the trench to interface with the light source and detector. POF was chosen due to its compatibility with the waveguide, as both share the same core material, PMMA, and have matching core dimensions [31]. Then, the trench on the PMMA sheet was carefully filled with the UPR solution. The UPR was then left to cure at room temperature for 24 hours. After hardening, the surface was refined using a cutter and P60 sandpaper, followed by sanding with acetone to smooth the surface. The fabricated waveguide surface was then examined using a Charge-Coupled Device (CCD) microscope.

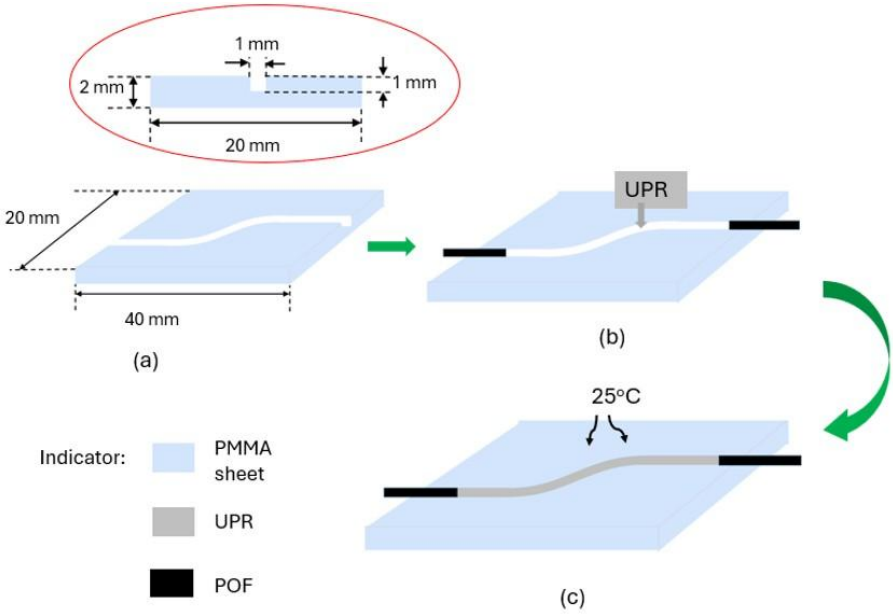

Figure 3. Waveguide fabrication process: (a) The S-bend groove was milled with a depth of 1 mm, (b) POF was attached at both ends of the trench, then the UPR solution was filled in the trench, and (c) the waveguide was cured at room temperature.

Sensor Characterization

The S-bend waveguide sensor was characterized by measuring the output power loss in response to temperature changes. A red-light source operating at a wavelength of 650 nm was used as the input, while a photodiode served as the detector. The sensor was immersed in distilled water, which was heated from 40 °C to 80 °C in 10 °C increments using a magnetic stirrer [29]. Measurement of the actual temperature was done by using a thermocouple embedded in the magnetic stirrer and displayed on its screen. The change in output intensity was recorded using an Arduino-based optical power meter, as shown in Figure 4. Each measurement was repeated six times to ensure repeatability and reliability. To evaluate hysteresis, the measurements were performed in two cycles: one with increasing temperature and another with decreasing temperature. For the response time analysis, the output intensity was recorded every five seconds over a 15-minute period for each temperature point.

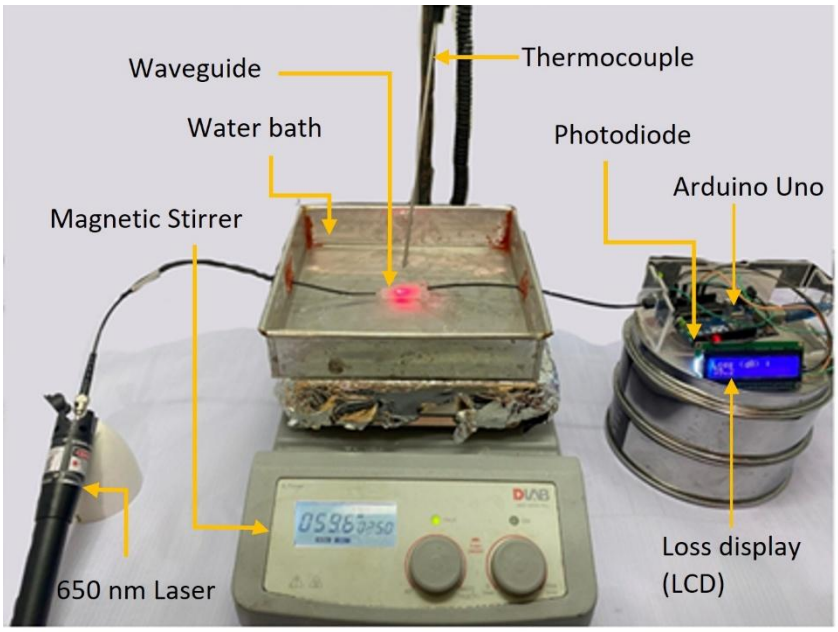

(a)

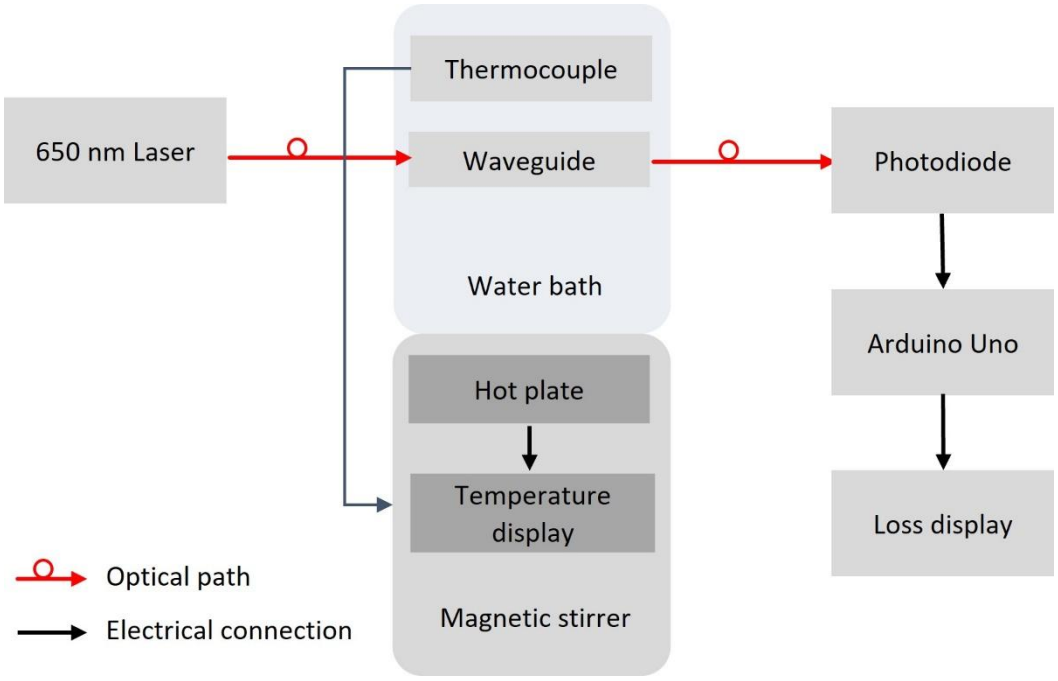

(b)

Figure 4. (a) Experimental setup of the waveguide temperature sensor using a 650 nm laser source, water bath with thermocouple and hot plate, and photodiode detection connected to Arduino for loss measurement. (b) Block diagram of optics and electronics showing data flow to the Arduino loss display and the temperature readout.

Result and Discussion

Waveguide Surface Quality and Dimension

The analysis of the CCD image confirmed that the core material (UPR) was evenly distributed within the PMMA cladding, with minimal surface roughness and air bubbles, as shown in Figure 5. A smooth core surface is crucial for minimizing scattering loss and improving light transmission efficiency [32]. Surface smoothness directly affects the propagation of light through the waveguide. Any surface irregularities or trapped air bubbles can lead to increased scattering and coupling loss, which reduces the overall sensor sensitivity and accuracy. A smooth core-cladding interface ensures that the evanescent field remains confined within the core, thereby enhancing light transmission efficiency and reducing bending loss.

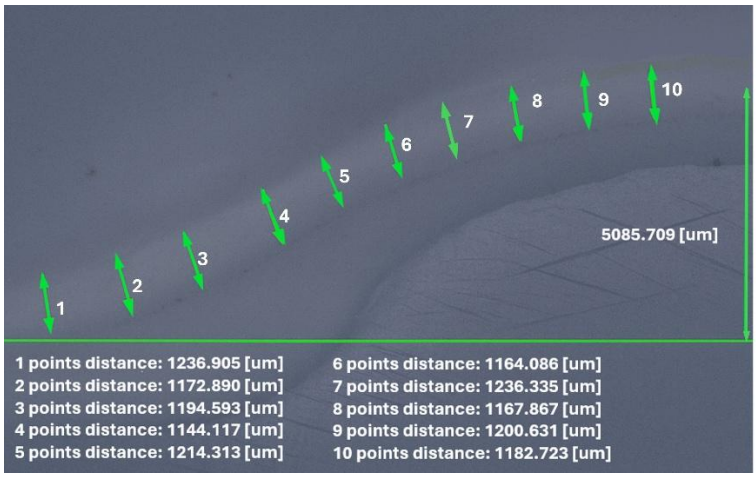

(a)

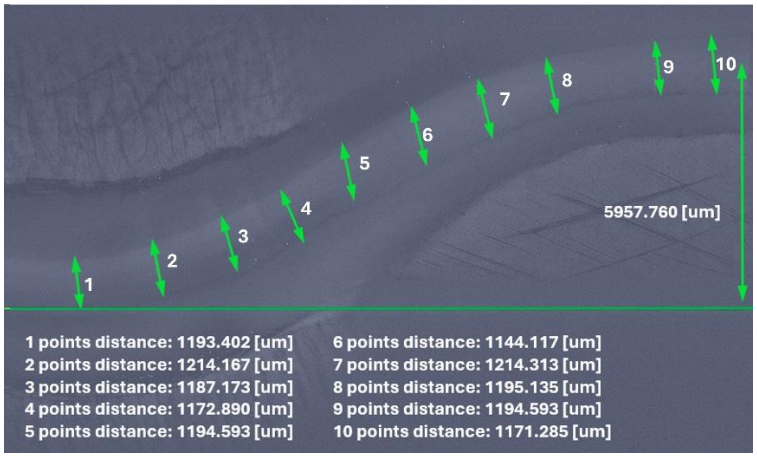

(b)

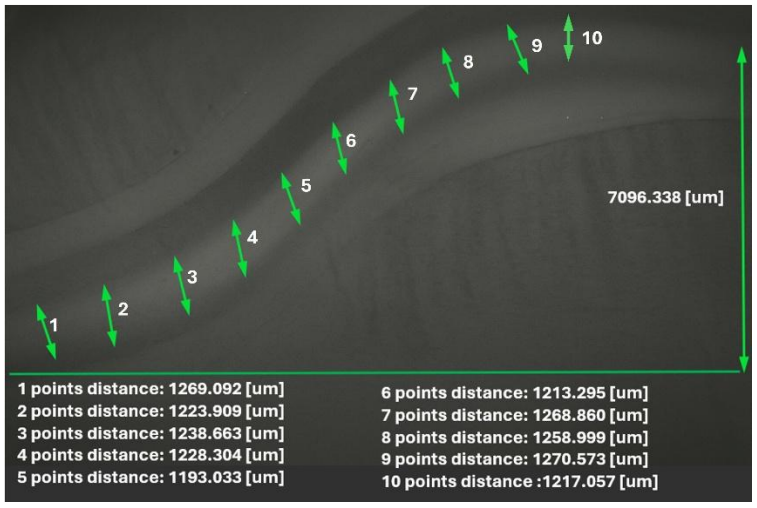

(c)

Figure 5. Microscope CCD images of S-bend waveguide with *h* of (a) 0.5 mm, (b) 0.6 mm and (c) 0.7 mm

The polishing and acetone treatment steps employed in this study proved effective in minimizing surface roughness. As observed in the CCD images in Figure 5, the core surface appears smooth and well-defined, with negligible visible defects or trapped air. This level of surface quality is essential for reducing propagation loss, especially in curved geometries such as S-bends, where light is more susceptible to escaping the core due to curvature-induced stress on the mode field. Studies have shown that even submicron-scale roughness (greater than 2 - 5 nm RMS) on waveguide surfaces can introduce measurable optical loss through Rayleigh scattering, particularly in polymer-based waveguides [33]. Therefore, the effective suppression of roughness through mechanical sanding and chemical smoothing is vital to achieving stable and high-performance waveguiding.

The CCD images in Figure 5 also provided a detailed dimensional analysis of the fabricated waveguides. Measurement errors were minimized by performing ten times measurements at different positions along the waveguide and ensuring consistent sample placement throughout the experiments. The measured bend heights and core widths for each sample are shown in Table 1. The average deviation from the designed values was within ±0.01 cm, which reflects the high precision of the CNC milling process.

Table 1. Comparison of designed and measured dimensions of S-bend waveguides.

Sample	Designed Bend Height (cm)	Measured Bend Height (cm)	Designed Core Width (mm)	Mean Core Width (mm)	Standard Deviation (μm)
1	0.5	0.508	1.0	1.191	31.03
2	0.6	0.596	1.0	1.123	21.02
3	0.7	0.709	1.0	1.240	35.81

As summarized in Table 1, the maximum standard deviation of the measured dimensions was 35.81 μm, corresponding to a 3% measurement error, which is within an acceptable tolerance for this type of measurement. This variation likely arises from minor inconsistencies during the CNC milling and curing processes. Nevertheless, the overall dimensional uniformity demonstrates that the fabrication process is both highly repeatable and precise. The reduced surface roughness and improved dimensional accuracy contribute to enhanced repeatability and long-term stability of the sensor's performance. Notably, previous studies have shown that polymer-based waveguides with smooth surfaces and precise dimensions exhibit improved thermal and mechanical stability under repeated thermal cycling [29].

Sensitivity and Linearity

The sensitivity of the S-bend waveguide sensor was evaluated by examining the relationship between output power loss and temperature variation, as illustrated in Figure 6. The results show a clear trend of increasing power loss with rising temperature, indicating that higher temperatures lead to greater optical attenuation [34]. This increase in power loss is primarily attributed to temperature-induced changes in the refractive indices of both the core and cladding materials, as well as the overall alteration of the waveguide's optical properties. A decrease in the cladding's refractive index results in a larger critical angle, which facilitates more efficient light transmission through the waveguide. Consequently, the optical transmittance increases, and power loss is reduced.

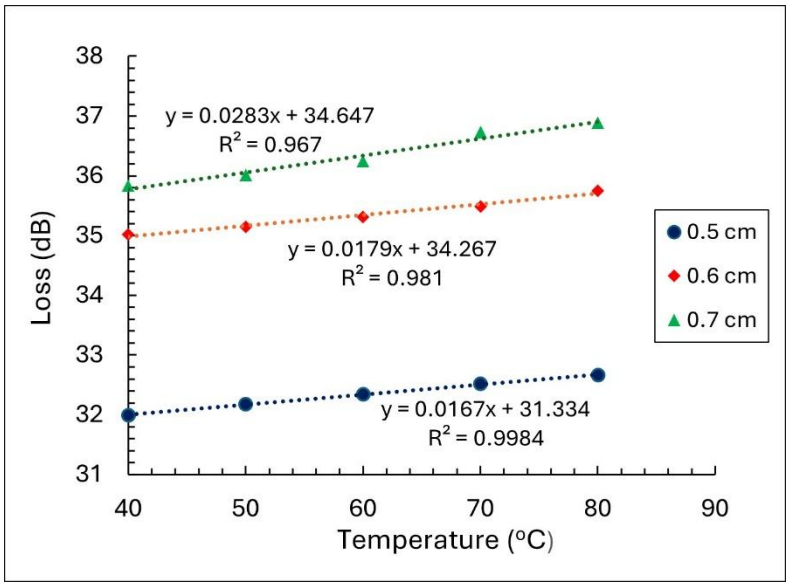

(a)

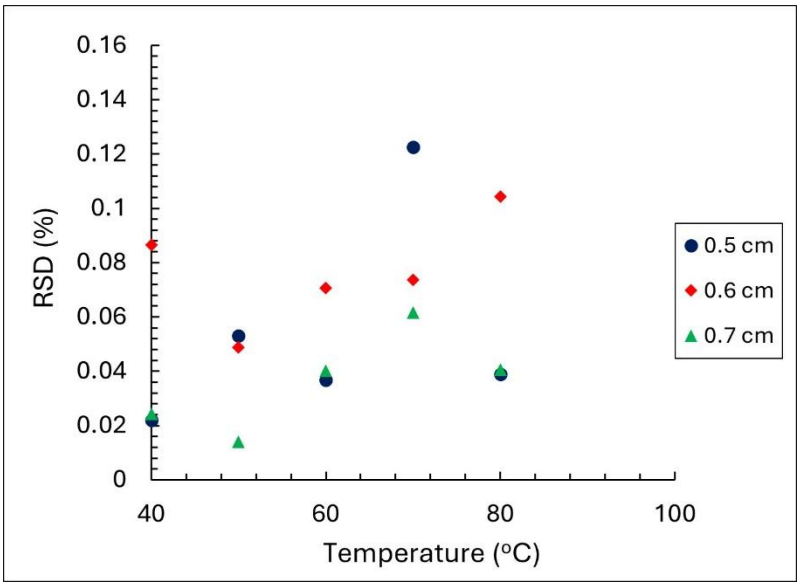

(b)

Figure 6. Power loss vs temperature variation of S-bend waveguide with *h* of 0.5 cm, 0.6 cm, and 0.7 cm (a) and the relative standard deviation (RSD) of the measurement for each sample (b).

Figure 6(a) shows that power loss varies linearly with temperature for all waveguides over the measured range. Based on the calculated slope of each curve, it is evident that sensitivity increases with greater bend height. For comparison, the sensitivities of various S-bend waveguides are summarized in Table 2. The highest sensitivity, measured at 0.0283 dB/°C, was achieved with a bend height of 0.7 cm, corresponding to a correlation factor of 96.7%. The observed increase in sensitivity with larger bend heights can be attributed to the enhanced interaction between the evanescent field and the core material, as well as the more pronounced influence of bending on light propagation within the waveguide. Compared to

straight waveguide in the previous study [28], the S-bend waveguide provides sensitivity improvement up to 217 %. Therefore, it confirms that the S-bend structure enhances evanescent field interaction and improves light confinement, providing a simple yet highly effective method for increasing sensor sensitivity.

Table 2. Sensitivity of S-bend waveguides with various bend height (h).

Bend Height (cm)	Sensitivity (dB/°C)	Correlation Factor (%)
0.5	0.0167	99.84
0.6	0.0179	98.10
0.7	0.0283	96.70

Bending in an optical waveguide creates a lateral shift in the light propagation path, causing part of the optical power to leak into the cladding due to reduced total internal reflection. In an S-bend structure, the bending introduces controlled coupling between the guided mode and the evanescent field at the core-cladding interface, which enhances the sensitivity to change in the refractive index caused by temperature variations. At higher bend heights, the curvature increases, which intensifies the evanescent field's penetration into the cladding region [33, 35]. This increased penetration leads to stronger interaction with the core material (UPR), whose refractive index is temperature dependent. The thermo-optic effect in UPR causes changing in the refractive index with temperature, modulating the light propagation through the waveguide and resulting in higher sensitivity. Mathematically, the bending loss in a curved waveguide is described by the following relation [30]:

$$\alpha = C_1 exp(-C_2 R) \quad (2)$$

where a is the bending loss, C_1 and C_2 are waveguide constants which depend on the waveguide and on the optical mode shape, and R is the bend radius (inversely related to bend height). The high sensitivity was also achieved due to the combination of a smooth core surface and precise waveguide dimensions. The smooth surface reduces scattering loss [32], while the consistent core width ensures stable light transmission and consistent evanescent field interaction.

Figure 6(b) presents the RSD for each S-bend waveguide sample. The RSD was employed as an indicator to assess the measurement repeatability and stability of the sensor performance across multiple experimental trials. A lower RSD value indicates higher consistency in the sensor's output and a more reliable measurement system. From the results, the maximum RSD values for the samples with bend heights of 0.5 cm, 0.6 cm, and 0.7 cm were found to be 0.123%, 0.104%, and 0.057%, respectively. The consistently low RSD values for all samples highlight the robust repeatability of the sensor, which is crucial for reliable temperature sensing applications.

To further improve sensitivity, future work could focus on reducing surface roughness at the core-cladding boundary to minimize scattering loss and optimize the refractive index contrast between core and cladding by experimenting with different polymer combinations or doping concentrations.

Response Time

Figure 7 shows the response time characteristics of each sample under identical sensing conditions. The response time is defined as the duration required for the sensor to reach 90% of its final output upon exposure to a stimulus. The response time of the S-bend waveguide sensor was consistently stable at approximately 40 seconds across all variations of bend height. The response time of 40 seconds achieved in this study is typical for polymer-based sensors [36] but slower than silica-based sensors.

Response time is influenced by several key factors, including the thermal conductivity of the core and cladding materials, the thickness of the waveguide, and the efficiency of light propagation through the core-cladding interface. The response time of an optical sensor is primarily determined by the thermal conductivity and thermo-optic properties of the materials used. UPR is a polymer with moderate thermal conductivity (0.28 W/m·K) [37]. Similarly, the thermal conductivity of PMMA falls within a comparable range to that of UPR, approximately 0.167 to 0.25 W/m·K [38]. This implies that while PMMA contributes to light confinement and low scattering loss, it also restricts the rate of heat transfer, thereby limiting the sensor's response speed, which explains why the response time is slower compared to silica-based sensors. However, the benefit of this slower response is greater stability and reduced noise in the sensor signal [39].

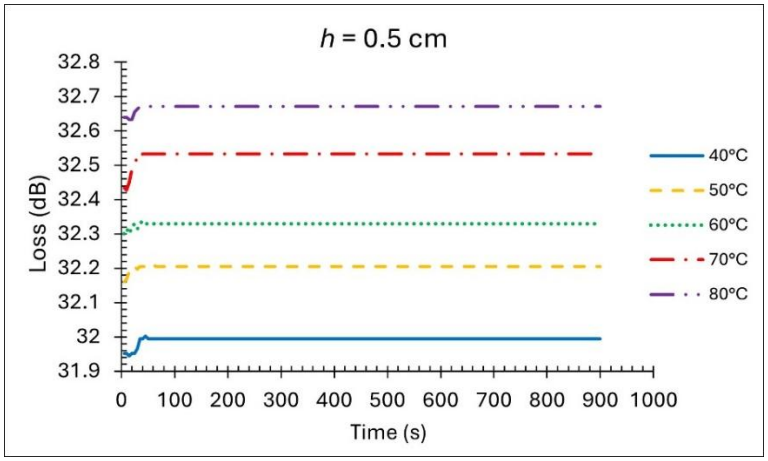

(a)

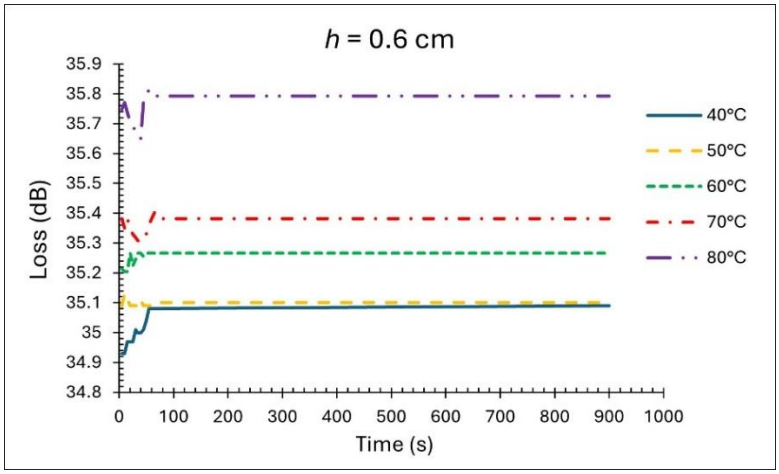

(b)

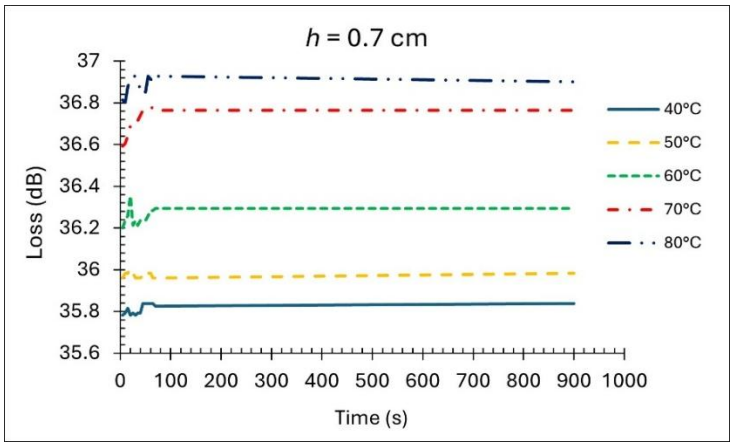

(c)

Figure 7. Response times of S-bend waveguide with bend height of (a) 0.5 cm, (b) 0.6 cm, and (c) 0.7 cm.

The slower response time in this study reflects the trade-off between sensitivity and response speed. The increased sensitivity due to higher evanescent field penetration comes at the cost of longer response time due to the lower thermal conductivity of the polymer materials. To improve response time without sacrificing sensitivity, the following approaches can be explored: using core materials with higher thermal conductivity and reducing the cladding thickness to allow faster heat exchange between the core and the environment.

Hysteresis

The hysteresis behavior of the S-bend waveguide sensor is presented in Figure 8 for each bend height. Hysteresis (H) is a critical parameter in temperature sensor performance because it indicates the sensor's ability to maintain consistent readings during repeated heating and cooling cycles. It is defined as the maximum difference in loss between the heating and cooling cycles at the same temperature point, as defined by [40]

$$H = \mathrm{Max}\left|\left(I(i) - D(i)\right) * 100\%/I(i))\right| \quad (3)$$

where $I(i)$ and $D(i)$ are the loss from the increasing cycle and the decreasing cycle of the i^{th} data, respectively.

The hysteresis values for the sensors with bend heights of 0.5 cm, 0.6 cm, and 0.7 cm were 0.118 %, 0.144 %, and 0.202 %, respectively. These values were all within an acceptable range, indicating that the sensor structure maintains consistent optical properties even under repeated thermal cycling. This consistency is likely due to the good thermal stability of the PMMA/UPR materials, as reported in previous studies [29]. The relatively low hysteresis confirms that the sensor design provides stable and reliable performance with minimal drift or memory effects. The hysteresis observed in this study is primarily attributed to minor thermal expansion mismatches between the core and cladding materials, as well as light power fluctuations.

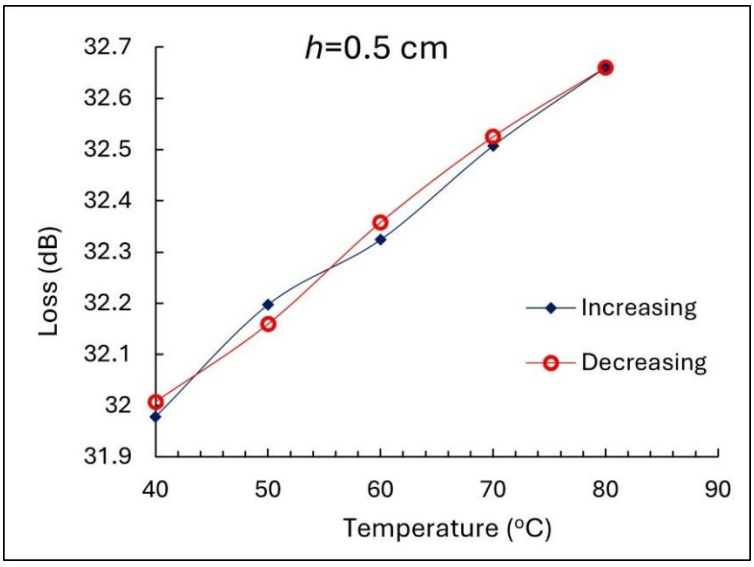

(a)

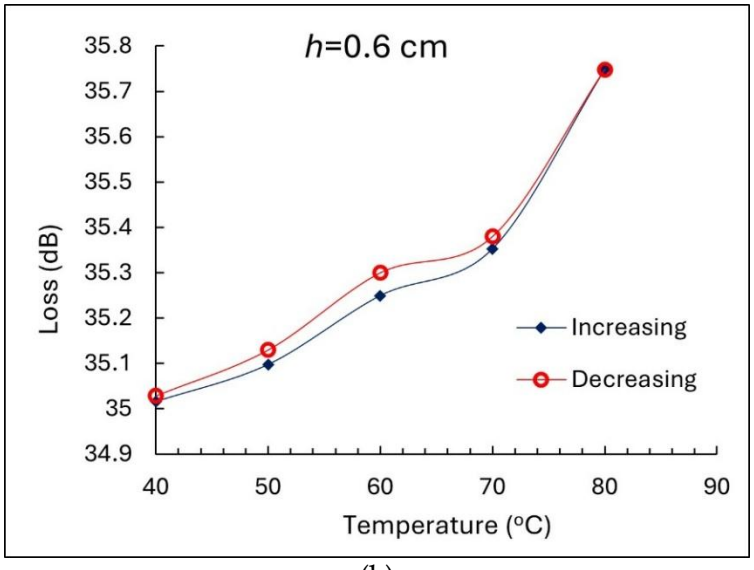

(b)

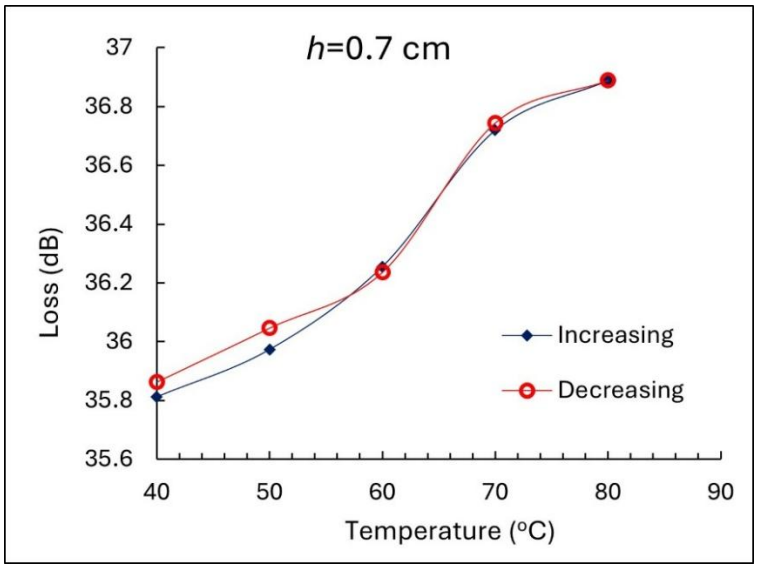

(c)

Figure 8. Hysteresis behavior of S-bend waveguide sensor with h of (a) 0.5 cm, (b) 0.6 cm, and (c) 0.7 cm.

Accuracy

The accuracy of the sensors is tabulated in Table 3. The accuracy was calculated using the following equation:

$$Accuracy = \frac{(1-\text{Average deviation})\times 100\%}{\text{Full span}} \qquad (4)$$

The highest accuracy of 99% was achieved at a bend height of 0.5 cm. Accuracy in an optical sensor is defined as the ability of the sensor to provide an output that closely matches the true value of the measured parameter. In this study, accuracy was influenced by propagation loss, coupling efficiency, and consistency of the evanescent field interaction. Accuracy tends to decrease at higher bend heights due to increased bending loss and light leakage into the cladding. At smaller bend heights (e.g., h = 0.5 cm), the waveguide maintains stronger light confinement and lower scattering loss, which ensures a more stable and predictable output signal. The accuracy of 99% achieved at h = 0.5 cm is comparable to other optical fiber temperature sensors [41].

Table 3. Accuracy of S-bend waveguide temperature sensors for various bend heights.

Bend height (cm)	Actual Temp. (°C)	Measured Temp. (°C)	Real error	Average deviation	Accuracy (%)
0.5	40	39.457	0.543		
	50	50.554	0.554		
	60	60.301	0.301	0.552	99.31%
	70	70.796	0.796		
	80	79.433	0.567		
0.6	40	42.186	2.186	1.881	97.65%

	50	49.072	0.928		
	60	58.337	1.663		
	70	68.102	1.898		
	80	82.730	2.730		
0.7	40	42.054	2.054		
	50	48.149	1.851		
	60	56.488	3.512	2.374	97.03%
	70	73.665	3.665		
	80	79.210	0.790		

Conclusion

This research successfully demonstrates the development of a polymer-based sine S-bend waveguide sensor for temperature measurement using a straightforward CNC milling fabrication method. The sensor's performance was evaluated based on its sensitivity, response time, accuracy, and hysteresis across different bend heights. The highest sensitivity of 0.0283 dB/°C was achieved at a 0.7 cm bend height, while the best accuracy of 99.31% was recorded at 0.5 cm. The response time remained stable at approximately 40 seconds across all samples. The maximum hysteresis observed was 0.202 % at a bend height of 0.7 cm, confirming the sensor's stable performance during repeated thermal cycling. These findings highlight the advantages of using a sine S-bend structure combined with accessible polymer materials to develop a low-cost, reliable, and scalable temperature sensor. Future work may focus on optimizing the polymer composition to further enhance the sensor's performance and evaluating the long-term stability.

Acknowledgment

We would like to thank the Faculty of Mathematics and Natural Sciences, Universitas Negeri Semarang, for funding the research through grant number 023.17.2.690645/2024.04/2024. Our gratitude also goes to the members of the Physics Department, Universitas Negeri Semarang for their helpful discussion throughout the completion of this work.

References

[1] R. Soltani Sarvestani, R. Ghayour, and M. Mohitpour, "Design and analysis of an optical demultiplexer based on Bragg grating using plasmonic waveguides and defects," *Optik*, vol. 322, p. 172209, 2025.

[2] Z. Wang, J. Du, K. Xu, and Z. He, "Wideband non-degenerate two-photon absorption in low-loss multimode silicon waveguides for nonlinear optical tuning between C and 2-μm wavebands," *Opt. Commun*, vol. 578, p. 131506, 2025, doi: 10.1016/j.optcom.2025.131506.

[3] J. Zhang and Q. Chen, "A Ti: LiNbO3 optical waveguide sensor for measurement of intensive electric field," *Opt. Laser Technol*, vol. 169, p. 110091, 2024.

[4] P. K. Teotia and R. S. Kaler, "Multilayer with periodic grating-based high-performance SPR waveguide sensor," *Opt. Commun*, vol. 395, pp. 154–158, Jul. 2017.

[5] B. Hooda and V. Rastogi, "Low cost highly sensitive miniaturized refractive index sensor based on planar waveguide," *Optik*, vol. 143, pp. 158–166, Aug. 2017.

[6] G. Mamtmin, P. Nizamidin, R. Abula, and A. Yimit, "Composite optical waveguide sensor based on porphyrin@ZnO film for sulfide-gas detection," *Chin. J. Anal. Chem*, vol. 51, no. 7, p. 100260, 2023

[7] Y. Tan et al, "Slit shaping technique for femtosecond laser direct write fabrication of two-dimensional symmetric waveguide arrays in silica glass," *Opt. Laser Technol*, vol. 182, p. 112146, 2025.

[8] P. A. Mohammed, R. M. Abdulla, and S. B. Aziz, "Light-matter interaction during and post polymerization in self-written polymer waveguide integrated with optical fibers," *Phys. B Condens. Matter*, vol. 695, p. 416481, 2024.

[9] Z. Gao et al, "Silica–Polymer Heterogeneous Hybrid Integrated Mach–Zehnder Interferometer Optical Waveguide Temperature Sensor," *Polymers*, 2024.

[10] H. Deng et al, "A Temperature Sensor Based on Composite Optical Waveguide," *J. Light. Technol*, vol. 40, no. 8, pp. 2663–2669, 2022. [Online]. Available: https://opg.optica.org/jlt/abstract.cfm?URI=jlt-40-8-2663

[11] R. B. Davila et al, "Printed Optical Waveguide Temperature Sensor With Rhodamine-Doped Core," *IEEE Sensors Lett*, vol. 8, no. 8, pp. 1–4, 2024, doi: 10.1109/LSENS.2024.3420781.

[12] R. M. Silva et al, "A simple, self-referenced, intensity-based optical fibre sensor for temperature measurements," *Opt. Commun*, vol. 291, pp. 215–218, Mar. 2013.

[13] J. Li et al, "An optical fiber temperature sensor based on fluorescence intensity ratio in Er3+/Yb3+ co-doped Gd2O3 phosphors," *Ceram. Int*, vol. 49, no. 17, Part B, pp. 28913–28919, 2023.

[14] X. Wang, S. Chen, S. Xu, and L. Chen, "Dual-mode optical thermometers and optical fiber temperature sensor based on La2MoO6: Er3+, Yb3+ phosphors," *J. Lumin*, vol. 280, p. 121096, 2025.

[15] M.-H. Yu et al, "The development of a dual-mode optical temperature sensor based on fluorescence intensity ratio and lifetime," *Ceram. Int*, vol. 50, no. 7, Part B, pp. 11766–11775, 2024.

[16] X. Jiao, X. Gong, and Z. Guo, "X-LiNbO3/sapphire optical temperature sensor based on light field manipulation," *Sensors Actuators A Phys*, vol. 387, p. 116357, 2025.

[17] M. Remouche, R. Mokdad, A. Chakari, and P. Meyrueis, "Intrinsic integrated optical temperature sensor based on waveguide bend loss," *Opt. Laser Technol*, vol. 39, no. 7, pp. 1454–1460, 2007.

[18] M. Remouche, F. Georges, and P. Meyrueis, "Flexible Optical Waveguide Bent Loss Attenuation Effects Analysis and Modeling Application to an Intrinsic Optical Fiber Temperature Sensor," *Opt. Photonics J*, vol. 2, no. 1, pp. 1–7, 2012.

[19] C. Gu, B. Li, X. Zuo, and Y. Liang, "Dual-core fiber temperature sensor based on bending assist and spot pattern demodulation," *Opt. Commun*, vol. 572, p. 130961, 2024.

[20] Y. Su et al, "S-shaped tellurite optical fiber surface plasmon resonance sensor for temperature and refractive index measurement," *Opt. Laser Technol*, vol. 179, p. 111385, 2024.

[21] S. P. K. Anguluri et al, "The design, analysis, and simulation of an optimized all-optical AND gate using a Y-shaped plasmonic waveguide for high-speed computing devices," *J. Comput. Electron*, vol. 20, 2021.

[22] N. Zamhari and A. A. Ehsan, "Large cross-section rib silicon-on-insulator (SOI) S-bend waveguide," *Optik*, vol. 130, pp. 1414–1420, 2017.
[23] S. Serecunova et al., "Waveguide shape and waveguide core size optimization of Y-branch optical splitters up to 128 splitting ratio," *Opt. Commun*, vol. 501, p. 127362, 2021.
[24] H. Zhao et al, "WMS-based near-infrared on-chip acetylene sensor using polymeric SU8 Archimedean spiral waveguide with Euler S-bend," *Spectrochim. Acta A Mol. Biomol. Spectrosc*, vol. 302, p. 123020, 2023.
[25] D.-H. Kim et al, "Novel S-Bend Resonator Based on a Multi-Mode Waveguide with Mode Discrimination for a Refractive Index Sensor," *Sensors*, 2019.
[26] Y.-J. Kim et al, "Thermal Reflow Effect in Multi-Mode Waveguide of S-Bend Resonator With Mode Discrimination," *IEEE Photonics J.*, vol. 14, no. 1, pp. 1–6, 2022.
[27] K. Srivastava and N. Bhatia, "Field propagation method in a square core optical waveguide for designing multimode interference devices," in Frontiers in Optics + Laser Science 2022 (FIO, LS), Rochester, NY, USA: Optica Publishing Group, 2022, p. JW5B.34. [Online]. Available: https://opg.optica.org/abstract.cfm?URI=LS-2022-JW5B.34
[28] Yulianti et al, "Performances characterization of unsaturated polyester resin/polymethylmethacrylate waveguide for refractive index measurement," *Optik*, vol. 242, p. 167305, 2021.
[29] Yulianti et al, "Thermal Durability Characterization of a Simple Polymethyl-methacrylate (PMMA)," *J. Penelit. Fis. dan Apl*, vol. 14, no. 2, pp. 113–124, 2024.
[30] Syahriar, "Improved S-bend optical waveguide loss formula verified by experiments," *Sci. Rep*, vol. 15, no. 1, p. 1338, 2025.
[31] W. Hardiantho, B. Arminah, and A. Arifin, "Detection of Mercury Ions in Water Using a Plastic Optical Fiber Sensor," *Indones. Phys. Rev*, vol. 4, no. 2, pp. 95–103, 2021.
[32] N. F. Mohd Ibrahim et al, "Surface roughness effect on optical loss in waveguide using isotropically induced crosslink network of siloxane–polyimide copolymer," *J. Appl. Polym. Sci*, vol. 137, no. 47, p. 49554, 2020.
[33] M. S. Ab-Rahman et al, "Optimum design of an optical waveguide: Determination of the branching angle of s-bend waveguides," *Optik*, vol. 200, p. 163249, 2020.
[34] V. Prajzler and J. Zázvorka, "Polymer large core optical splitter 1×2 Y for high-temperature operation," *Opt. Quantum Electron*, vol. 51, no. 7, p. 216, 2019.
[35] F. Brik, S. Harize, A. Fares, and K. Saouchi, "Offset effect on the S-Bend structure losses and optimization of its size for integrated optics," *Int. J. Electr. Comput. Eng*, vol. 10, no. 4, pp. 4162–4167, 2020.
[36] Luo et al, "Analytical Evaluation and Experiment of the Dynamic Characteristics of Double-Thimble-Type Fiber Bragg Grating Temperature Sensors," *Micromachines*, vol. 12, no. 1, 2021.
[37] N. Bing et al, "Unsaturated polyester resin supported form-stable phase change materials with enhanced thermal conductivity for solar energy storage and conversion," *Renew. Energy*, vol. 173, pp. 926–933, 2021.
[38] M. Rohde et al, "Intercomparison of thermal diffusivity measurements on CuCrZr and PMMA," *High Temp. Press*, vol. 42, 2014.
[39] J. Casanova-Chafer, "Advantages of Slow Sensing for Ambient Monitoring: A Practical Perspective," *Sensors*, vol. 23, 2023.

[40] M. S. Avila-Garcia et al., "High sensitivity strain sensors based on single-mode-fiber core-offset Mach-Zehnder interferometers," *Opt. Lasers Eng*., vol. 107, pp. 202–206, 2018.

[41] J. Li et al, "High-accuracy distributed temperature measurement using difference sensitive-temperature compensation for Raman-based optical fiber sensing," *Opt. Express*, vol. 27, no. 25, pp. 36183–36196, 2019.